

INFLUENCE OF CRYSTAL STRUCTURE ON MOLECULAR STRUCTURE: SYNTACTIC STRUCTURAL CHEMISTRY

EDWARD R. T. TIEKINK

Department of Chemistry, National University of Singapore, Singapore 117543. E-mail: chmtert@nus.edu.sg

A discussion dealing with the influence of crystal packing requirements upon molecular geometry for a series of mercury dithiolates and organotin systems is presented in this overview. Firstly, the remarkable structural diversity, with changes in coordination numbers and geometries, will be demonstrated for two series of mercury dithiolates and a for series of triorganotin carboxylates. The potential to form hypervalent interactions, either intra- or intermolecularly, is crucial in allowing the adoption of different motifs. Qualitative explanations based on the necessity of satisfying the bonding requirements of the central element and the need to maximise intermolecular interactions will be put forward to account for the different motifs found in the solid-state. Finally, the powerful combination of crystallography and *ab initio* molecular orbital calculations will be illustrated. In this way, the influence of the crystalline environment upon molecular geometry can be quantified. In summary, the molecules described in this overview adopt geometries that are *synthatic* with their host environment.

Introduction

Two key issues confront chemical crystallographers when they analyse and present their structural data. First and foremost, what relevance do the structural results have to the solution structure? In macromolecular chemistry, where the crystals are often composed of significant amounts of solvent, usually water, it may be argued that the structural data bears some resemblance to the solution structure. However, in chemical crystallography, where the incorporation of solvent can and indeed does occur, but not normally to the same extent as in macromolecular structures, the molecules cannot be considered as solvated as perhaps for macromolecular crystallography. Rather than being surrounded by solvent, molecules are immersed in an ordered environment defined by other molecules. This environment is often thought of as being inert in terms of influencing, to a significant extent, the molecular geometry. Perhaps the only exception to this rule of thumb is in cases where hydrogen-bonding interactions impose conformational preferences. The premise that the crystalline manifold is inert in the sense of not imposing significant structural changes in molecules is the assumption underlying *crystal engineering*, *i.e.* the rational design of molecular solids by tailoring intermolecular interactions. In this way, a *supramolecular synthon* is designed with a specific pattern of intermolecular

functionality in mind and crystallised to form a specific array of molecules. But, what would happen if the host environment exerted an influence on the molecular structure of the synthon so that significant changes occurred from the crystal engineer's drawing board to reality. This account will present some examples of series of structures where major changes in structure occur, changes that are ascribed to the influence of crystal packing requirements. In this way, the second major issue confronting chemical crystallographers is addressed: what influence does the crystal structure exert on molecular structure?

In the first part of this account, a series of mercury thiolate structures will be described as will an attempt to rationalise the observed structural diversity. Attention will then be directed to some organotin compounds. A qualitative explanation for structural diversity for a series of triorganotin carboxylates will be given. Finally, a summary of recent work correlating experimental and theoretical structures with the view of obtaining a quantitative understanding of the influence of crystal packing forces on molecular structure will be given.

Mercury(III) Bis(1,1-thiolates)

Owing to their wide use in various industrial and commercial applications, the structural chemistry of the zinc triad 1,1-dithiolates has attracted considerable attention over the years. If there is

one series of structures that underpin the issues described above in the *Introduction*, it is the structures found for the mercury(II) bis xanthates, *i.e.* $\text{Hg}(\text{S}_2\text{COR})_2$, $\text{R}=\text{Me}$ [1], Et [2], iPr [3] (Scheme 1). The remarkable structural diversity for these compounds is fascinating and defies conventional explanation. A brief overview of three structural motifs is presented below.

A representation of the crystallographically determined structure of $\text{Hg}(\text{S}_2\text{COMe})_2$ is illustrated in Fig. 1. It is immediately apparent from this diagram that there are distinct coordination modes for the xanthate ligands. One is bidentate bridging, linking neighbouring mercury atoms into a helical chain, and the other is monodentate as the pendant sulfur atom is not involved in coordination to mercury. The coordination geometry is one based on a T-shape. The apparently simple substitution of the methyl substituents of $\text{Hg}(\text{S}_2\text{COMe})_2$ by ethyl groups leading to $\text{Hg}(\text{S}_2\text{COEt})_2$, results in a profound change in

structure. As emphasised by the mercury atom indicated with an asterisk in Fig. 2, all xanthate ligands are bridging so that the mercury atoms now exist in four-coordinate, distorted tetrahedral geometries. Also, as noted from the lower left-hand portion of Fig. 2, the structure is constructed about 16-membered rings comprising four mercury atoms and four bidentate bridging xanthate ligands. The layer structure that results is an assembly of interconnected 16-membered rings, *i.e.* $-\text{[Hg-S-C-S]}_4-$. Further substitution of the ethyl groups in $\text{Hg}(\text{S}_2\text{COEt})_2$ by isopropyl groups giving $\text{Hg}(\text{S}_2\text{COiPr})_2$, again results in a significant change in structure. The 16-membered $-\text{[Hg-S-CS]}_4-$ rings of $\text{Hg}(\text{S}_2\text{COEt})_2$ persist in the structure of $\text{Hg}(\text{S}_2\text{COiPr})_2$ as shown in Fig. 3. In this structure there are both chelating and bidentate bridging xanthate ligands. This has the result that for each of the asterisked mercury atoms in Fig. 3, two sulfur atoms derived from a chelating xanthate ligand define the distorted tetrahedral ge-

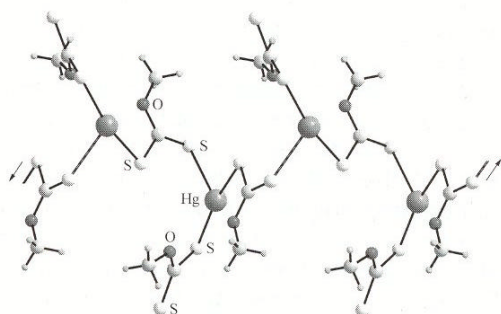


Fig. 1. Portion of the polymeric structure of $\text{Hg}(\text{S}_2\text{COMe})_2$.

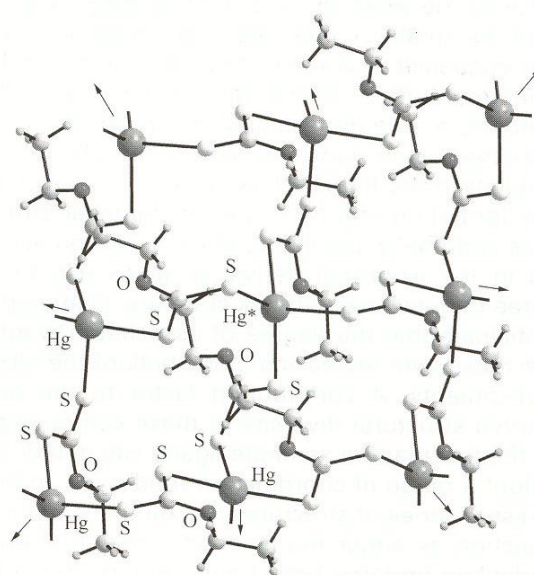


Fig. 2. Portion of the layer structure of $\text{Hg}(\text{S}_2\text{COEt})_2$.

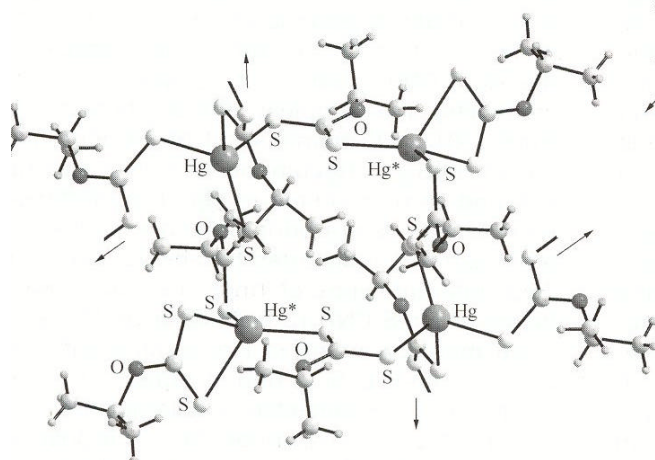
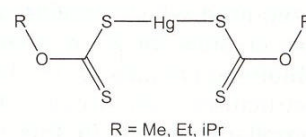


Fig. 3. Portion of the network structure of $\text{Hg}(\text{S}_2\text{COiPr})_2$.



Scheme 1. Chemical structure for $\text{Hg}(\text{S}_2\text{COR})_2$ pertaining to Figs. 1–3.

ometry along with two sulfur atoms derived from two bridging thiolate ligands. The remaining mercury atoms have tetrahedral coordination geometries similar to the mercury atoms in $\text{Hg}(\text{S}_2\text{COEt})_2$. In this structure, not all of the bridging xanthate ligands extend laterally to form a layer structure as described above for $\text{Hg}(\text{S}_2\text{COEt})_2$. Instead, only two of the bridging xanthate ligands bridge neighbouring 16-membered rings that are approximately coplanar with the ring shown in Fig. 3, one xanthate ligand bridges another ring above and the other, below this approximate plane through the 16-membered ring. This arrangement leads to the formation of a network structure.

From the foregoing, it is clear that the substitution of remote organic substituents in the xanthate ligand leads to an intriguing array of structural motifs. A simple relationship may be envisaged for the R=Me and Et structures in that the monodentate xanthate ligand in $\text{Hg}(\text{S}_2\text{COMe})_2$ now bridges neighbouring chains leading to a layer structure. No obvious relationship between the structure of $\text{Hg}(\text{S}_2\text{COiPr})_2$ and the smaller congeners is apparent. Indeed, the sequence of complexity of the structures is counter-intuitive in that for the smallest substituent, a one-dimensional chain structure is observed. Increasing the size of the alkyl substituent in the thiolate ligand to ethyl results in the formation of a two-dimensional layer structure and finally, branching at the α -carbon atom as in the isopropyl derivative gives rise to a three-dimensional network structure. One might anticipate that the degree of association would decrease with increasing steric bulk of the alkyl substituents. A contributing factor to the observed structural diversity in these compounds is the fact that the xanthate ligand can and does adopt a range of coordination modes [4]. In the present series of structures the xanthate ligands function as either monodentate, chelating and bidentate bridging ligand and, importantly, one or more of these modes can be found within the same structure.

To rationalise the structural diversity in these and related systems a systematic structural study is required which implies the availability of suitable crystals for X-ray analysis. Unfortunately, obtaining crystals for the $\text{Hg}(\text{S}_2\text{COR})_2$ series of structures has proven difficult [5]. A more compliant system in this regard is one based on the

chemical structure shown in Scheme 2, i.e. $\text{Hg}(\text{S}_2\text{CNR}_2)_2$, the mercury(II) bis dithiocarbamates. Thus far, this system has revealed five distinct structural motifs but, importantly, a detailed examination of the crystal and molecular structures allows a proposal to account for the observed structural diversity [6]. The following discussion will be limited to the structures of archetypical examples for $\text{Hg}(\text{S}_2\text{CNR}_2)_2$ motifs, where R = iBu [6], Me [7], Et [8], nBu [6] and H [9], with full details for other derivatives summarised in the literature [6]. This will be followed by an overview of the rationale put forward to explain the appearance of the different motifs.

Unlike the previously described mercury bis(xanthate) structures, the overwhelming number of mercury(II) bis(dithiocarbamate) structures are isolated monomeric or dimeric species. The mercury atom in $\text{Hg}(\text{S}_2\text{CNiBu}_2)_2$ [6], illustrated in Fig. 4, is in a four coordinate geometry best described as distorted tetrahedral. This geometry arises as a result of a chelating mode of the dithiocarbamate ligand. A four coordinate geometry is also found for the structure of $\text{Hg}(\text{S}_2\text{CNMe}_2)_2$ [7] as shown in Fig. 5 but, this time, the coordination geometry is based on a square-planar geometry. There are weak $\text{Hg}\cdots\text{S}$ interactions above and below the square-plane but these distances are considered too long to represent significant bonding interactions. Dimeric motifs are found in the two structures illustrated in Figs. 6 and 7. In each of these there are two chelating and two bidentate bridging dithiocarbamate ligands. The mercury centres again exist in distorted tetrahedral geometries. For centrosymmetric $\text{Hg}(\text{S}_2\text{CNEt}_2)_2$ [8], the two bridging dithiocarbamate ligands are orientated in opposite directions. The dimeric unit of $\text{Hg}(\text{S}_2\text{CNiBu}_2)_2$ [6] is disposed about a crystallographic two-fold axis of symmetry indicating that the two bridging dithiocarbamate ligands lie to one side of the molecule. The final structure to be described for the $\text{Hg}(\text{S}_2\text{CNR}_2)_2$ series of compounds is that containing the simplest dithiocarbamate, i.e. $\text{Hg}(\text{S}_2\text{CNH}_2)_2$ [9]. Reminiscent of the aforementioned $\text{Hg}(\text{S}_2\text{COEt})_2$ compound, a layer structure is found as represented in Fig. 8. All dithiocarbamate ligands are bridging and each mercury atom exists in a distorted tetrahedral geometry. Two different types of rings are found within layers of $\text{Hg}(\text{S}_2\text{CNH}_2)_2$. Focussing on the asterisked mercury atoms in Fig. 8, an eight-membered

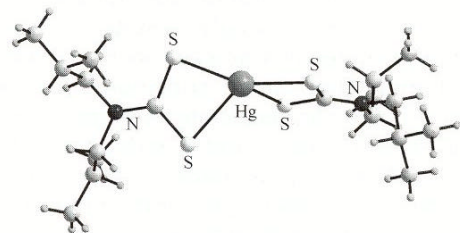


Fig. 4. The monomeric structure of $\text{Hg}(\text{S}_2\text{CNIiBu})_2$.

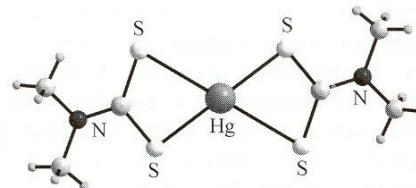


Fig. 5. The monomeric structure of $\text{Hg}(\text{S}_2\text{CNMe})_2$.

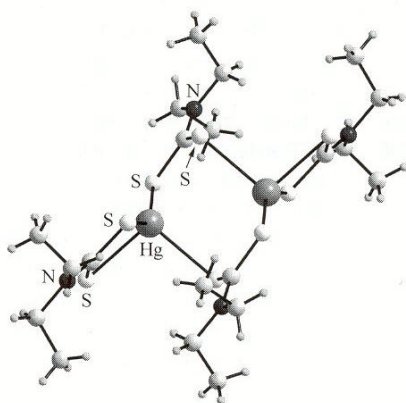


Fig. 6. The dimeric structure of $\text{Hg}(\text{S}_2\text{CNEt})_2$.

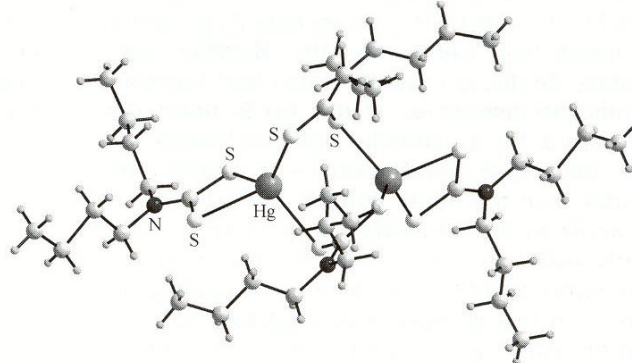


Fig. 7. The dimeric structure of $\text{Hg}(\text{S}_2\text{CNnBu})_2$.

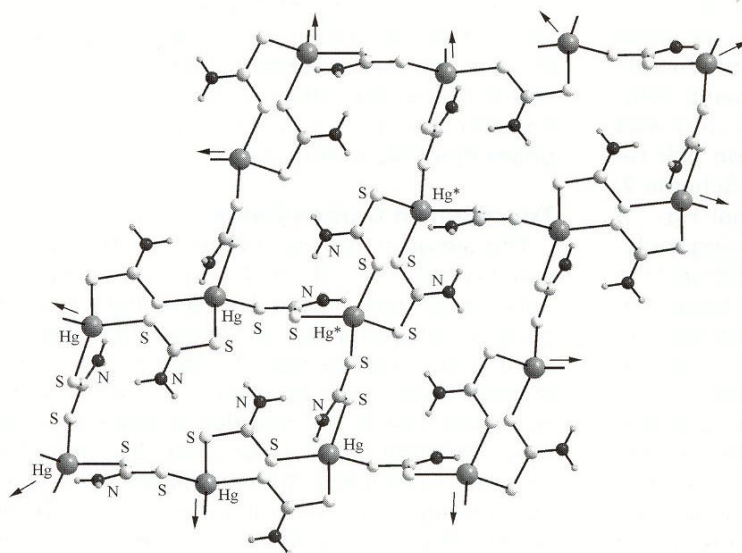
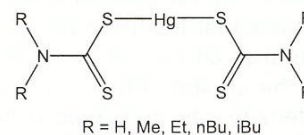


Fig. 8. The layer structure of $\text{Hg}(\text{S}_2\text{CNH}_2)_2$.



Scheme 2. Chemical structure for $\text{Hg}(\text{S}_2\text{CNR})_2$ pertaining to Figs. 4–8.

–[Hg-S-C-S]–₂ ring is apparent. These rings are interconnected via larger 24-membered –[Hg-S-C-S]–₆ rings that comprise six mercury atoms. Another way of describing this motif is to define a network of interconnected 24-membered rings.

Within each 24-membered ring, each of two diagonally opposite pairs of mercury atoms is bridged by a dithiocarbamate ligand that serves to stabilise the otherwise flexible ring. Further stabilisation of the ring is afforded by intra-ring N-H...

S interactions.

It might be argued that the structural diversity in the $\text{Hg}(\text{S}_2\text{CNR}_2)_2$ compounds is not as dramatic as for the $\text{Hg}(\text{S}_2\text{COR})_2$ series. Nevertheless, the variety in structural motifs is remarkable remembering that the only change in the chemical composition of the $\text{Hg}(\text{S}_2\text{CNR}_2)_2$ compounds relates to the nature of the nitrogen-bound substituent, a substituent that does not participate in coordination to mercury. This point is highlighted by the fact that the $\text{Hg}(\text{S}_2\text{CNEt}_2)_2$ compound is known to adopt both the dimeric motif shown in Fig. 6 as well as the monomeric motif related to square-planar $\text{Hg}(\text{S}_2\text{CNMe}_2)_2$ [8, 10]. Despite this, a ‘first principle’ rationalisation for the appearance of different motifs has been made [6].

A close inspection of the derived interatomic parameters defining the mercury atom geometries in the $\text{Hg}(\text{S}_2\text{CNR}_2)_2$ series reveals a number of interesting trends for the R=alkyl compounds. Firstly, it must be noted that there are significant disparities in the Hg-S bond distances, i.e. for a particular dithiocarbamate ligand, one Hg-S bond distance is significantly shorter than the other. Further, the presence of an angle in the coordination geometry significantly wider than the ideal 90° (square-planar geometry) or 109.5° (tetrahedral) angles is apparent. In this context, it is salutatory to recall that the valency at mercury should be satisfied by two covalent Hg-S interactions so that the presence of more than two Hg-S bonds for mercury indicates that the Hg-S interactions in the Figures are weaker than conventional covalent bonds. Given the geometric data cited above, it is possible to conclude that the molecular structures may be regarded as being comprised of linear S-Hg-S groups in accord with the conventional valence shell electron pair repulsion model and as represented in Scheme 2, distortions notwithstanding. Additional $\text{Hg}\cdots\text{S}$ interactions occur to give rise to differing molecular aggregates. Taken to an extreme, the bonding around the mercury can be thought of being comprised two covalent interactions and two hypervalent interactions which can be either intra- (as for chelating dithiocarbamate) or inter-molecular (as for bidentate bridging dithiocarbamate). Of course, once the molecules are set in the crystal lattice, reorganisation of electron density can and does occur so as to optimise the mercury to sulphur interactions. In this way the distinction between formal covalent and hyperva-

lent interactions becomes blurred, and distortions in molecular geometry arise. The driving force behind the above is the axiom that the molecules will adopt positions in the crystal lattice so as to maximise their intermolecular interactions. So, why do monomeric and dimeric motifs arise? The answer is undoubtedly steric in origin. An increase in the steric profile of the dithiocarbamate ligands, i.e. the alkyl substituents, usually results in isolated tetrahedral molecules as seen in Fig. 4. On the other hand, when steric considerations allow, two molecules can associate to form a dimeric pair as seen in Figs. 6 and 7. Indeed, a detailed analysis of the crystal packing in monomeric $\text{Hg}(\text{S}_2\text{CNiBu}_2)_2$ shows that centrosymmetrically related pairs of tetrahedral molecules are orientated so as to, potentially, associate to form a dimeric unit related to that seen in Fig. 6. That there exists a close balance between the requirements to satisfy the bonding of the mercury atom and the dictate to optimise intermolecular interactions is emphasised by the appearance of two motifs (see above) for $\text{Hg}(\text{S}_2\text{CNEt}_2)_2$. Clearly, more work is required in order to rationalise the structural diversity observed in the mercury bis(xanthate) and bis(dithiocarbamate) structures. Indeed, a review [11] of the structural chemistry of the zinc triad elements with these and related ligands showed that there were eight distinct motifs for these compounds and new ones have been discovered since.

Subsequent work to be summarised in this overview relates to organotin compounds. There exists an interesting variability in the structural motifs for the triorganotin carboxylates and a rationale has also been proposed to account for this. Attention then is directed towards the examination of monomeric species and comparing the structures of these with gas-phase theoretical studies.

Triorganotin Carboxylates

The simplest representation of a triorganotin carboxylate, i.e. $\text{R}_3\text{Sn}(\text{O}_2\text{CR}')$, is shown in Scheme 3. Here, it can be seen that three organic substituents and an oxygen atom derived from a carboxylate ligand coordinating in the monodentate mode bind the tin atom. The ensuing discussion will describe a series of structures containing this basic structural unit. The tin atom in Scheme 3 has satisfied its valency by forming four covalent interactions and the structural variability

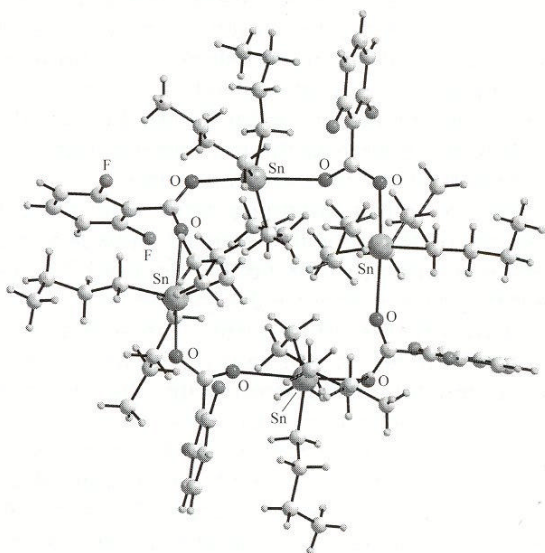


Fig. 9. The tetrameric structure of $n\text{Bu}_3\text{Sn}(\text{O}_2\text{CR}^1)$; see Scheme 3 for the chemical structure of HO_2CR^1 .

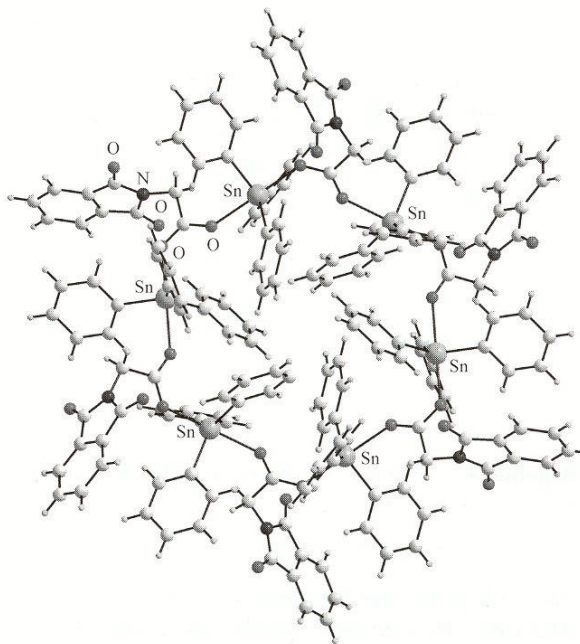


Fig. 10. The hexameric structure of $\text{Ph}_3\text{Sn}(\text{O}_2\text{CR}^2)$; see Scheme 3 for the chemical structure of HO_2CR^2 .

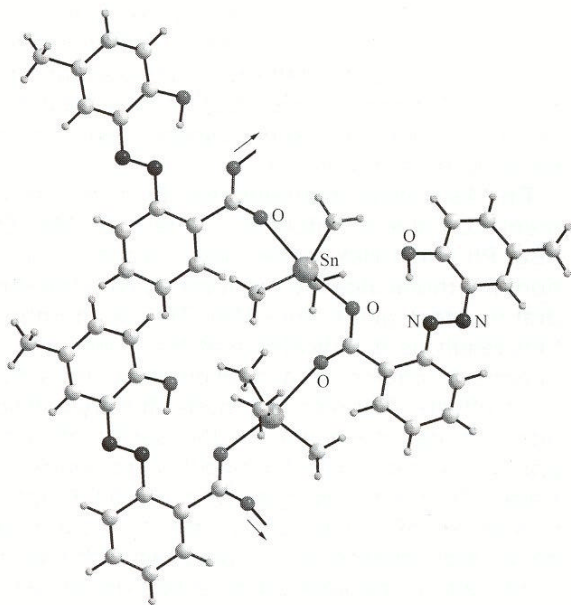


Fig. 11. The polymeric structure of $\text{Me}_3\text{Sn}(\text{O}_2\text{CR}^3)$; see Scheme 3 for the chemical structure of HO_2CR^3 .

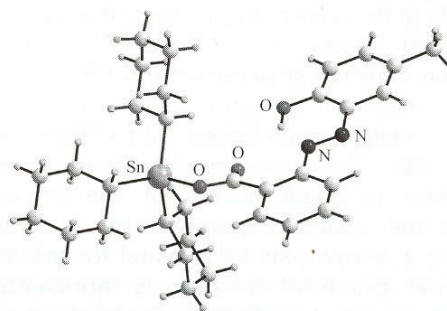
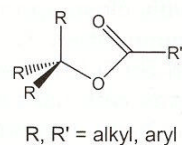


Fig. 12. The monomeric structure of *c*- $\text{Hex}_3\text{Sn}(\text{O}_2\text{CR}^3)$; see Scheme 3 for the chemical structure of HO_2CR^3 .

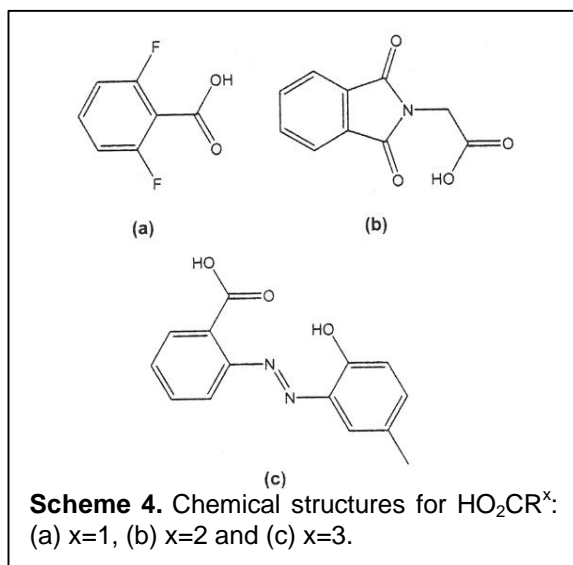


Scheme 3. Chemical structure for $\text{R}_3\text{Sn}(\text{O}_2\text{CR}')$ pertaining to Figs. 9–12.

about to be described differs in the mode of association of the 'non-coordinating' oxygen atom. As above, the additional interactions between tin and the carbonyl oxygen atom, either intra- or intermolecular, are hypervalent or secondary interac-

tions.

As represented in Fig. 9, 16-membered $-\text{[Sn-O-C-O-]}_4$ rings, reminiscent of those found in some of the mercury(II) bis xanthate structures described above, are found in the structure of



$\text{R}_3\text{Sn}(\text{O}_2\text{CR}^1)$ [12]; see Scheme 4 for the chemical structure of HO_2CR^1 . In this structure each successive pair of tin atoms is bridged by a bidentate bridging carboxylate ligand. This has the result that each tin atom is five-coordinate, existing in a distorted trigonal bipyramidal geometry in which the trigonal plane is defined by three carbon atoms. An even larger, 24-membered ring comprising six tin atoms is found in the structure of $\text{R}_3\text{Sn}(\text{O}_2\text{CR}^2)$ [13] as shown in Fig. 10; see Scheme 4 for the structure of HO_2CR^2 . This arises, again, as a result of bidentate bridging carboxylate ligands. The oligomeric structures shown in Figs. 9 and 10 are in fact oddities, there being only one example of each in the literature. The remaining compounds of this class adopt one of the two motifs described below for $\text{R}_3\text{Sn}(\text{O}_2\text{CR}^3)$ [14]; see Scheme 4 for the structure of HO_2CR^3 . A portion of the polymeric structure of $\text{Me}_3\text{Sn}(\text{O}_2\text{CR}^3)$ is shown in Fig. 11; see Scheme 4 for the structure of HO_2CR^3 . The now familiar five-coordinate geometry is again found for the tin atoms within the chain propagated by a crystallographic 2_1 -screw axis as is usual for this motif. The final structural variation is represented in Fig. 12 for $c\text{-Hex}_3\text{Sn}(\text{O}_2\text{CR}^3)$. By contrast to the structures described above, the structure is monomeric with the tin atom existing in a distorted tetrahedral geometry. The distortion from the ideal tetrahedral geometry may be traced in part to the relatively close approach of the pendant carbonyl oxygen atom. Compounds of the general formula $\text{R}_3\text{Sn}(\text{O}_2\text{CR}')$ form an important class of com-

pounds with uses in industry, agriculture and, potentially, in medicine. As such, many structural studies have been published for these compounds over the last 30 years or so. However, the lack of a systematic analysis in terms of systematically varying the nature of the tin-bound substituents or of the carboxylate ligand has precluded a rationalisation for the adoption of the polymeric over the monomeric motif.

The system containing the carboxylate ligand derived from HO_2CR^3 did furnish crystals for $\text{R}=\text{Me}$, Et, nBu, Ph and $c\text{-Hex}$. Thus, a series of structures were obtained where the carboxylate ligand was held constant and the nature of the R_3Sn moiety altered. A careful and systematic analysis of the crystal structures as well as an appreciation of the hypervalent interactions allowed a qualitative rationalisation for the adoption of the polymeric (i.e. for $\text{R}=\text{Me}$, Et and nBu) motif in preference to the monomeric motif (i.e. $\text{R}=\text{Ph}$ and $c\text{-Hex}$) for these structures.

The clue to this quandary came from the calculation of the repeat distances between successive tin atoms in the polymeric motif. The repeat distance is about 5.0 Å for the three structures with $\text{R}=\text{Me}$, Et and nBu. The similarity of these distances is not surprising as geometric parameters associated with the bridging $-\text{O}-\text{C}-\text{O}-$ functionality are basically constant and the variations in the Sn-O distances, while influenced by the nature of the tin-bound organic substituents, do not vary significantly. As described above, such polymeric arrays are not found in the $\text{R}_3\text{Sn}(\text{O}_2\text{CR}^3)$ structures with $\text{R}=\text{Ph}$ and $c\text{-Hex}$. However, a similar calculation determining the repeat distance between successive tin atoms reveals that the distance, while greater than 5.0 Å, is approximately the same. This key result allows a qualitative description of the crystallisation process for the $\text{R}_3\text{Sn}(\text{O}_2\text{CR}^3)$ compounds. Before this model is described one key spectroscopic experiment needs to be summarised.

Tin-119 nuclear magnetic resonance measurements on the $\text{R}_3\text{Sn}(\text{O}_2\text{CR}^3)$, where $\text{R}=\text{Me}$, Et, nBu, Ph and $c\text{-Hex}$, series showed that in solution, the molecules are monomeric with tetrahedral tin atom geometries [14]. This is an important result as it indicates that the formation of polymeric chains is a consequence of solid-state effects. A molecular model for crystallisation can be envisaged for the series of compounds in that isolated

molecules are deposited from solution at distances of about 5.0 Å apart, regardless of the nature of the tin-bound organic substituents. In keeping with the basic principles of the packing of solids (molecules), the tetrahedral molecules make the necessary adjustments to minimise free space in the lattice by maximising their intermolecular interactions. In the case of the R=Me, Et and nBu compounds, this is achieved by forming hypervalent, intermolecular Sn...O interactions leading to the polymeric motif. For the R=Ph and c-Hex structures, such intermolecular hypervalent interactions are not possible owing to the steric bulk of the tin-bound substituents. A hypervalent Sn...O interaction is still formed but, intramolecularly not intermolecularly. It is argued that the adoption of different motifs for this particular series of structures relates to steric factors associated with the triorganotin centres and again, the dictates of efficient crystal packing result in different molecular structures. In crystal engineering terms, the $R_3Sn(O_2CR^3)$ synthon aggregates via directional Sn...O interactions in one motif and non-directional hydrophobic interactions in the monomeric motif.

The qualitative explanations for the range of motifs found for the mercury(II) bis dithiocarbamates and triorganotin carboxylates notwithstanding, greater satisfaction is gained by quantitative analyses. This can be achieved by resorting to theoretical calculations. In this way, the experimental, i.e. crystallographically determined, structure is compared with the theoretical structure, i.e. that obtained by *ab initio* molecular orbital calculations. In essence, one is comparing the results of the solid-state structure with a gas-phase structure, i.e. a structure in the absence of crystal packing effects. Assuming that the theoretical model is appropriate, the differences between the experimental and theoretical structures may be ascribed to the influence of intermolecular forces operating in the former. The comparison of monomeric species is particularly useful in this context and so the remaining part of this account will focus on monomeric organotin systems.

As indicated above, it is imperative to establish an appropriate protocol for the theoretical calculations. This was achieved by comparing the geometric results obtained from calculations for small organotin species with those from experimental structures determined by both single crys-

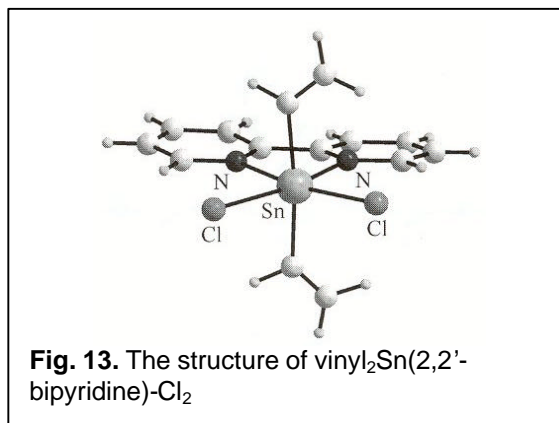


Fig. 13. The structure of vinyl₂Sn(2,2'-bipyridine)-Cl₂

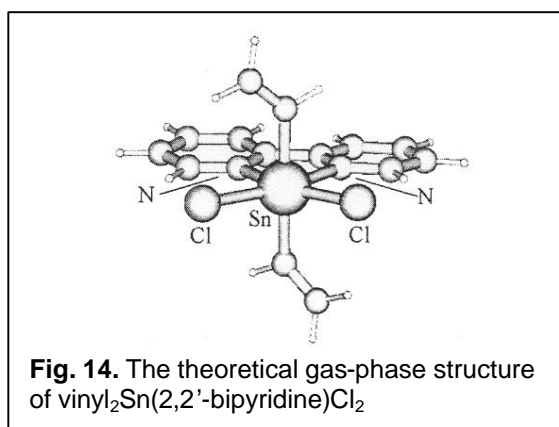
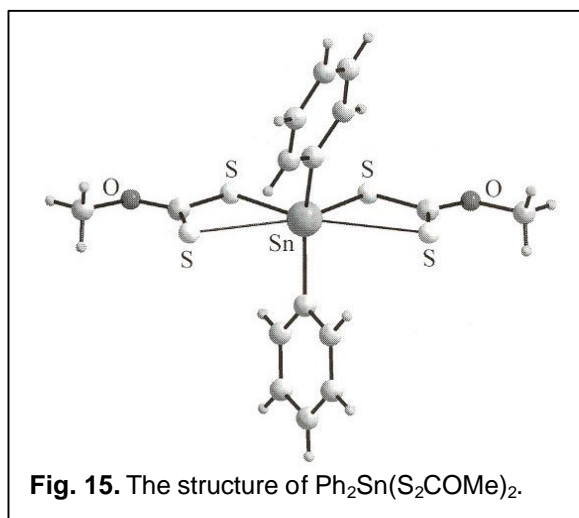


Fig. 14. The theoretical gas-phase structure of vinyl₂Sn(2,2'-bipyridine)Cl₂

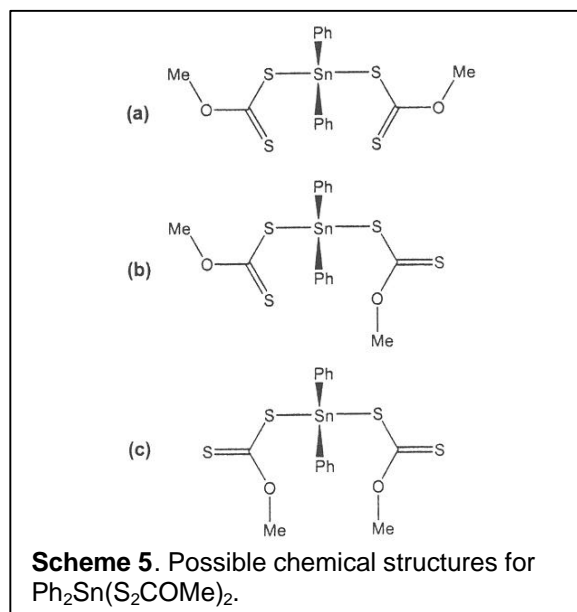
tal X-ray diffraction and electron diffraction methods. A comparison of molecular geometries and derived interatomic parameters were paramount in selecting a theoretical model and basis set for subsequent calculation [15]. An example of an experimental structure is shown in Fig. 13, i.e. vinyl₂Sn(2,2'-bipyridine)Cl₂, where vinyl is C(H)=CH₂. The tin atom in this structure (that crystallised as a benzene hemi-solvate) exists within a C₂Cl₂N₂ ligand donor set and the coordination geometry is distorted octahedral. There is no crystallographically imposed symmetry in the structure but there is an approximate mirror plane relating the two vinyl entities. Taking this structure as a starting point, geometry optimisation calculations were performed. Put another way, the molecule was 'isolated' from its crystal packing environment and allowed to adjust its coordination geometry until a global energy-minimised structure was obtained.

A view of the energy-minimised structure calculated for vinyl₂Sn{2,2'-bipyridine}Cl₂ is represented in Fig. 14. The obvious difference between



Figs. 13 and 14 relates to the disposition of the vinyl groups. The approximate mirror symmetry in the experimental structure has optimised to a structure with 2-fold symmetry. As a consequence, the inequivalent pairs of Sn-Cl, Sn-N and Sn-C bond distances found in the crystal structure are now the same. Thus, in the absence of a crystal packing influence, there has been a change in the molecular geometry accompanied by a symmetrisation of the structure. This is a general result obtained from such calculations. For example, molecules with two independent molecules in the asymmetric unit (crystallographic isomers) converge to the one energy-minimised structure and in the same way, differences observed in polymorphic systems are removed upon geometry optimisation. Further, where the chemistry allows, chemically equivalent bond distances that are experimentally distinct in the crystal structure become equivalent in the optimised structure. These key results point to the influence of the crystal-packing manifold upon the molecular structure at least in the compounds investigated [15]. The challenge now is to try and get quantitative data, i.e. to determine the energy of stabilisation associated with crystal packing.

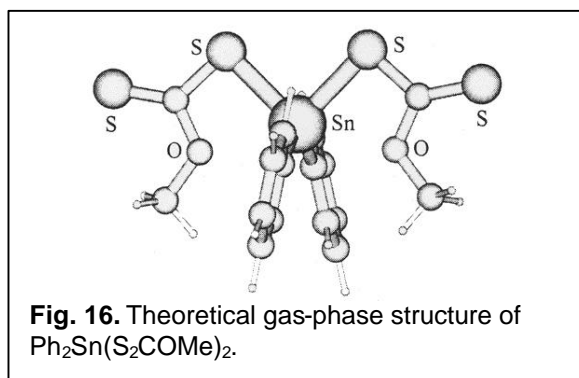
One way of obtaining this information would be determine the energy difference between the geometry-optimised and experimental (i.e. a single point calculation) structures. The difference in energy could be regarded as a reflection of the energy of stabilisation associated with crystal packing. The problem with this approach is that there are always experimental errors in the X-ray



crystallographic experiment, most notably in the hydrogen atom positions that usually modelled so as to account for electron density. In addition, the theoretical model also introduces assumptions as to the electronic structure of the molecule under investigation. Also, in the X-ray experiment a vibrationally averaged structure is determined as opposed to the equilibrium structure calculated by *ab initio* methods. The above has been redressed somewhat in the following example which has allowed a more reliable estimate of the energy of stabilisation associated with crystal packing.

The molecular structure of $\text{Ph}_2\text{Sn}(\text{S}_2\text{COMe})_2$ is illustrated in Fig. 15 [16]. Two phenyl groups and two xanthate ligands coordinate the tin atom in this structure. The xanthate ligands adopt a chelating mode but form asymmetric tin to sulphur interactions. The formal valency of tin would be satisfied by four covalent bonds and so the weaker of the Sn-S bonds may be considered as intramolecular hypervalent interactions. The coordination geometry is best described as being based on a skew-trapezoidal bipyramidal arrangement of a C_2S_4 donor set. In this description the tin-bound phenyl groups are disposed so as to lie over the hypervalent tin to sulphur interactions.

In keeping with the idea that the tin to sulphur interactions are hypervalent, it is apposite to consider other potential donor atoms within the xanthate ligand. These are, of course, the oxygen atoms. Indeed, tin can be regarded, in terms of the



hard acid/soft base concept, as a hard acid and thus, would be expected to form a hypervalent interaction with a hard oxygen atom rather than a soft sulphur atom. With this in mind it is possible to envisage three structures that differ in the nature of their hypervalent interactions. These options are illustrated in Scheme 5. The structure in Scheme 5(a) represents the crystallographically determined structure of $\text{Ph}_2\text{Sn}(\text{S}_2\text{COMe})_2$ that features two hypervalent $\text{Sn}\cdots\text{S}$ interactions. A rotation about the covalently bound sulphur-carbon bond now places the oxygen atom in close proximity to tin and makes available the thione sulphur for intermolecular interactions as shown in Scheme 5(b). In Scheme 5(c), both oxygen atoms are in position to form hypervalent interactions to tin. So, what did the theoretical calculations indicate for this system?

The geometry-optimised structure for $\text{Ph}_2\text{Sn}(\text{S}_2\text{COMe})_2$ is illustrated in Fig. 16. It is evident from this Figure that there has been a significant change from the experimentally observed structure as the optimised geometry resembles the geometry shown in Scheme 5(c) with the formation of two hypervalent $\text{Sn}\cdots\text{O}$ interactions. The question must be posed: which of the two structures is correct. Of course, the answer is that they are both correct! Remember that the two structures are isomers found in different phases. The theoretical structure is in keeping with conventional hard acid/soft base considerations as mentioned above. However, if this structure were translated directly into the solid-state, two electronegative thione groups would be presented for intermolecular interactions. In the event, a structure shown in Fig. 15 is found in which the more electronegative oxygen atoms are presented to neighbouring molecules allowing the formation of stronger intermolecular interactions. The ultimate

structure adopted in the solid-state is clearly determined by the joint considerations of satisfying valency and maximising intermolecular interactions. Importantly, this system affords the opportunity of investigation of the energetics associated with crystal packing.

Deliberately perturbing the experimental structure (Fig. 15) so as to adopt conformations illustrated in Schemes (b) and (c), and optimising all three structures gives a set of energy-minimised structures with that shown in Fig. 16, being the global minimum. The energy difference between the global minimum (Fig. 16) and the energy-minimised structure corresponding to that shown in Scheme 5(a), can be regarded as energy of stabilisation, provided by the crystalline manifold. This energy difference was determined to be approximately 20 kJ mol^{-1} , a value similar to that estimated for organic molecules [17]. Put another way, to enable the structure shown in Fig. 15 to be observed in the solid-state rather than that corresponding to Fig. 16, at least this amount of energy is required to stabilise the unstable conformation.

Conclusion

In this account it has been demonstrated, at least for the systems described, that structural diversity in very closely related compounds may be found that is both fascinating and intriguing. It is likely that the source of the variability in the structures can be traced to crystal packing effects operating upon these molecules in the solid-state. Primarily these are intra- and/or inter-molecular hypervalent interactions. The adoption of one particular structural motif over another appears to be dictated by the dual requirements of satisfying the valency requirements of the central element and maximising intermolecular interactions. Thus, it may be concluded that the molecular structures are syntactic with their host manifold and that significant adjustments in molecular geometry can be traced to the influence of crystal packing.

Acknowledgements

Much of the work described in this contribution was conducted whilst the author was at The University of Adelaide and funding from the Australian Research Council is gratefully acknowledged. The participation of students and colleagues, as indicated by the names in the reference listing, in this project is very much appreciated.

Crystallographic analyses were performed on Rigaku AFC6R and AFC7R diffractometers, the later fitted with the remarkably reliable X-Stream low temperature device. Structure analyses as described in this overview can not be performed automatically and thereby the author relied heavy on teXsan. In this context it is a pleasure to acknowledge the expert (and patient) technical advice provided by Dr Bev R. Vincent. The National University of Singapore (R-143-QQ-151-112) provides on-going support for this research.

References

- [1] E. R. T. Tiekink, *Acta Crystallogr.*, **1987**, C43,448.
- [2] (a) Y. Watanabe, *Acta Crystallogr.*, **1977**, 833, 3566;
(b) C. Chieh and K. J. Moynihan, *Acta Crystallogr.*, 1980, 836, 1367.
- [3] Y. Watanabe, *Acta Crystallogr.*, **1981**, 837, 553.
- [4] E. R. T. Tiekink and G. Winter, *Rev. Inorg. Chem.*, 1992, 12,183.
- [5] M. J. Cox and E. R. T. Tiekink, *Z. Kristallogr.*, 1999, 214, 486.
- [6] M. J. Cox and E. R. T. Tiekink, *Z. Kristallogr.*, 1999, 214, 571.
- [7] M. J. Cox and E. R. T. Tiekink, *Z. Kristallogr.*, 1997, 212, 542.
- [8] H. Iwasaki, *Acta Crystallogr.*, 1973, 829, 2115.
- [9] C. Chieh and S. K. Cheung, *Can. J. Chem.*, 1981, 59, 2746.